

REPORTS

quently harden the coat. However, this coating method is easily generalized to allow for different ways of hardening the particle coats. With the use of appropriate reagents, this technique is also compatible with schemes that thermally or optically initiate the hardening of the coats. Figure 6 shows confocal images of a polystyrene bead encapsulated with an agarose coat that was hardened by lowering its temperature. In Fig. 7, we show an optical micrograph of a poppy seed encapsulated in a poly(styrenesulfonic acid) coat that was photopolymerized. The selective withdrawal geometry may also be inverted by inserting the straw through the bottom of the withdrawal container, with the straw tip positioned below the interface. Now the denser aqueous fluid is the primary fluid being withdrawn, and the particles to be coated are placed in the oil (upper fluid). This inversion extends the applicability of this coating technique to hydrophobic particles in oil-soluble reagents as well as to heavy particles in the upper fluid that will sediment to the interfacial boundary.

The selective withdrawal coating technique complements other currently available techniques, such as surface-induced polymerization (10), which can also produce coats of uniform thickness on irregularly shaped particles but which often require modification of the particle surface and therefore may not be feasible. In our technique, as illustrated in the description of the polyamide coating, the particles can be completely separated from the caustic reagents that initiate the polymerization at the outer interface. Moreover, surface-induced polymerization requires the reagent to be stable in the solution being polymer-

ized. This is not always possible (as with the polyamide coat installation, the trichloride reagent is unstable in aqueous solutions), and selective withdrawal can solve this problem by initiating polymerization with a reagent that is stable in the fluid surrounding the coat. Finally, many polymer coatings are either difficult [e.g., the photopolymerized poly(styrenesulfonic acid) coat shown in Fig. 7] or impossible (e.g., the thermally hardened agarose coat shown in Fig. 6) to prepare using techniques such as surface-induced polymerization and must be hardened in bulk. For these cases in particular, selective withdrawal presents a valuable advantage over currently available coating techniques.

The selective withdrawal technique can be readily optimized. With a single tube we estimate that 10,000 particles can be coated per hour. Preliminary experiments have demonstrated that this technique can be scaled up by using an array of tubes in parallel. Injecting particles directly into the region below the spout can make the method suitable for particles with higher density than the prepolymer. As described above, inversion of the selective withdrawal geometry can extend the applicability of this technique to hydrophobic particles in oil-soluble reagents. Because of its flexibility in polymerization schemes, its ability to coat particles of many different types, and its ability to tune the thickness of the coats, this technique is an attractive option in a range of applications and a valuable addi-

tion to the repertoire of currently available coating techniques.

References and Notes

1. A. J. Mendonca, X. Y. Xiao, *Med. Res. Rev.* **19**, 451 (1999).
2. S. J. Shuttleworth, S. M. Allin, P. K. Sharma, *Synthesis* **11**, 1217 (1997).
3. F. Lim, A. M. Sun, *Science* **210**, 908 (1980).
4. P. Soon-Shiong, *Adv. Drug Deliv. Rev.* **35**, 259 (1999).
5. R. Langer, *Acc. Chem. Res.* **33**, 94 (2000).
6. G. H. J. Wolters, W. M. Fritschy, D. Gerrits, R. Van Schillegaarde, *J. Appl. Biomater.* **3**, 281 (1992).
7. T. Yoshioka, R. Hirano, T. Shioya, M. Kato, *Biotechnol. Bioeng.* **35**, 66 (1990).
8. E. Mathiowitz, *Encyclopedia of Controlled Drug Delivery* (Wiley, New York, 1999).
9. E. Donath, G. B. Sukhorukov, F. Caruso, S. A. Davis, H. Mohwald, *Angew. Chem. Int. Ed.* **37**, 2202 (1998).
10. G. M. Cruise, O. D. Hegre, D. S. Scharp, J. A. Hubbell, *Biotechnol. Bioeng.* **57**, 655 (1998).
11. J. R. Lister, *J. Fluid Mech.* **198**, 231 (1989).
12. S. Blake and G. N. Ivey, *J. Volcanol. Geotherm. Res.* **27**, 153 (1986).
13. I. Cohen and S. R. Nagel, in preparation.
14. E. E. Timm, U.S. Patent 4,444,961 (1984).
15. Even without the inclusion of particles, as originally shown by Savart [*Annal. Chim.* **53**, 337 (1883)] and Rayleigh [*Philos. Mag.* **34**, 177 (1892)], the prepolymer spout will break into droplets that can be hardened, allowing the fabrication of monodisperse particles.
16. A. M. Ganan-Calvo, *Phys. Rev. Lett.* **80**, 285 (1997).
17. P. B. Umbanhowar, V. Prasad, D. A. Weitz, *Langmuir* **16**, 347 (2000).
18. O. Valdes-Agullera, C. P. Pathak, J. Shi, D. Watson, D. C. Neckers, *Macromolecules* **25**, 541 (1992).
19. We thank H. Rilo and A. Rotamel for early discussions that motivated these studies. We also thank C. Lassy and the Confocal Digital Imaging Facility at the University of Chicago. Supported by NSF grant DMR-9722646 and NSF Materials Research Science and Engineering Centers Program grant DMR-9808595.

19 January 2001; accepted 7 March 2001

Anthropogenic Warming of Earth's Climate System

Sydney Levitus,^{1*} John I. Antonov,¹ Julian Wang,²
Thomas L. Delworth,³ Keith W. Dixon,³ Anthony J. Broccoli³

We compared the temporal variability of the heat content of the world ocean, of the global atmosphere, and of components of Earth's cryosphere during the latter half of the 20th century. Each component has increased its heat content (the atmosphere and the ocean) or exhibited melting (the cryosphere). The estimated increase of observed global ocean heat content (over the depth range from 0 to 3000 meters) between the 1950s and 1990s is at least one order of magnitude larger than the increase in heat content of any other component. Simulation results using an atmosphere-ocean general circulation model that includes estimates of the radiative effects of observed temporal variations in greenhouse gases, sulfate aerosols, solar irradiance, and volcanic aerosols over the past century agree with our observation-based estimate of the increase in ocean heat content. The results we present suggest that the observed increase in ocean heat content may largely be due to the increase of anthropogenic gases in Earth's atmosphere.

Studies using instrumental data to document a warming of Earth's climate system due to increasing concentrations of greenhouse gases (GHGs) have focused on surface air temperature and sea surface temperature (*T*).

These variables have proved invaluable for documenting an average warming of approximately 0.6°C at Earth's surface (*T*) during the past 100 years. Recent comparisons (2–4) with paleoclimatic proxy data indicate that

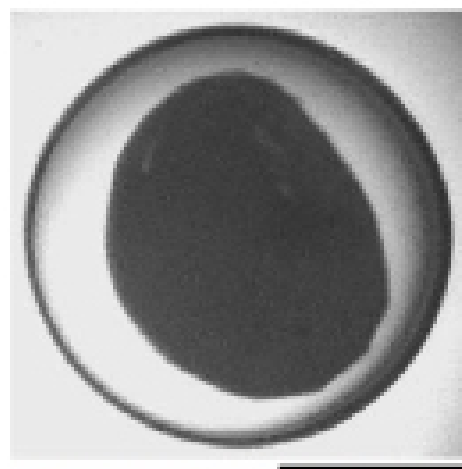


Fig. 7. Optical micrograph of a poppy seed encapsulated in a poly(styrenesulfonic acid) coat. The poppy seed appears as a dark solid object 0.9 mm in diameter; the coat is 0.2 mm thick. The prepolymer used is styrene sulfonic acid sodium salt (30% w/v in D₂O) and triethylene glycol diacrylate (5% w/v in D₂O) mixed with eosin Y (0.5 mM) and triethanolamine (100 mM) as the photosensitizer–electron donor initiating system (18). After the selective withdrawal process, the coated particles were collected in a plastic container and irradiated for 20 min with a halogen lamp. Scale bar, 0.5 mm.

REPORTS

the observed increase in surface temperature during the past century is unprecedented during the past 1000 years. The results of these studies, in conjunction with similar results found using general circulation model (GCM) and energy balance model studies (5–8) that include forcing by the observed time-dependent increase in GHGs and sulfate aerosols, as well as changes in solar irradiance and volcanic aerosols, provide evidence that the warming of Earth's surface during the past few decades is of anthropogenic origin. Despite the agreement between models and observations, it is conceivable that some of the surface warming might be com-

pensated for by a cooling of other parts of Earth's climate system. Conversely, additional warming may be occurring in other parts of the climate system, such as the recently observed warming of the world ocean (9).

Here we address these issues by quantifying the primary components of the heat balance of the Earth system. We document a warming of Earth's climate system during the latter half of the 20th century, based on increases in the heat content of the atmosphere and ocean, as well as estimates of the total heat of fusion associated with the partial melting of several components of Earth's cryosphere. Further, we compare these changes with increases in ocean heat content simulated by an atmosphere-ocean GCM (AOGCM) that is forced with estimates of the radiative effects of observed temporal variations in atmospheric GHGs, the direct effect of sulfate aerosols, solar irradiance, and volcanic aerosols over the past century.

The estimated temporal variability of

global ocean and atmospheric heat content, based on instrumental data for the 1955–96 period, is shown in Fig. 1. The ocean heat content time series (calculated for the global ocean over the depth range from 0 to 3000 m) and its computation were recently described (9). The atmospheric sensible heat content is based on the National Centers for Environmental Prediction/National Center for Atmospheric Research (NCEP/NCAR) reanalysis fields (10). The ocean heat content curve is based on analyses of 5-year running composites of historical ocean data. The atmospheric heat content is shown as anomalies averaged for 1-year periods. Other components of atmospheric energy change, associated with changes in the latent heat of evaporation and geopotential height field, are an order of magnitude smaller than the change in sensible heat in the NCEP/NCAR analyses. The increase in observed ocean heat content is 18.2×10^{22} J (based on the linear trend for the 1957–1994 period but prorated to 1955–1996), whereas the increase in atmospheric heat content is more than an order of magnitude smaller: 6.6×10^{21} J.

The melting and freezing of land and sea ice are physical processes that can act as sources or sinks of heat with respect to the atmosphere and ocean components of Earth's climate system. On the basis of estimates of the changes in the areal extent, thickness, or volume of these components of Earth's cryosphere, we estimate the total latent heat of fusion (11–13) that corresponds to their partial melting since approximately 1950. Such estimates require additional assumptions, such as assigning a salinity and temperature to the sea ice that melted or estimating the total amount of ice that has melted. We document the assumptions made in each of our estimates of cryospheric change (Table 1). We emphasize that we make assumptions that will produce relatively high estimates of the total heat of fusion that can be associated with the melting of these parts of the cryosphere, and

¹National Oceanographic Data Center/National Oceanic and Atmospheric Administration (NOEC/NOAA),
²Air Resources Laboratory, NOEC/NOAA, E/OCs,
1315 East-West Highway, Silver Spring, MD 20910,
USA. ³Geophysical Fluid Dynamics Laboratory/NOAA,
Post Office Box 308, Princeton, NJ 08542, USA.
⁴To whom correspondence should be addressed. E-mail: slevitus@nodc.noaa.gov

Fig. 1. Time series of various components of the observed and simulated global heat content (units are 10^{22} J). The observed global (calculated over the depth range from 0 to 3000 m) ocean heat content (9) is shown in black; the open circles denote the observed global mean atmospheric heat content (10). The red curve denotes the ensemble mean global ocean heat content from a set of three simulations (experiment GSSV) using a coupled ocean-atmosphere model. The model incorporates estimates of the radiative effects of past changes in GHGs, sulfate aerosols, solar irradiance, and volcanic aerosols. The blue curve denotes the same for an additional set of three simulations (experiment GS), which is similar to experiment GSSV except that the radiative effects of changes in solar irradiance and volcanic aerosols are omitted. For the two model curves, their respective means for 1955–1996 were removed before plotting. Note that 1.5×10^{22} J equals 1 watt-year m^{-2} (averaged over the entire surface of Earth).

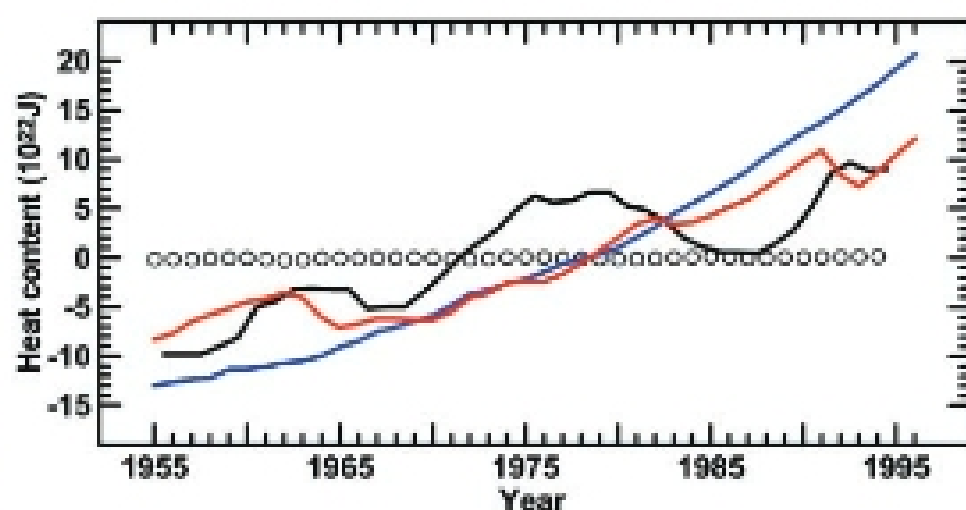


Table 1. Comparison of the heat balance of the climate system.

Component of the climate system and source of data	Time period of change	Observed or estimated change	Assumption made in this calculation	Heat content increase or total heat of fusion
World ocean (5)	1955–1996	Observed temperature increase	–	18.2×10^{22} J
Global atmosphere (6)	1955–1996	Observed temperature increase	–	6.6×10^{21} J
Decrease in the mass of continental glaciers (7)	1955–1996	–	Assumed 1.8 mm per year increase in sea level	8.1×10^{21} J
Decrease in Antarctic sea ice extent (18)	1950s–1970s	Estimated 311-km reduction in sea ice edge	$\rho_i = 9.17 \times 10^{11}$ kg km^{-3} $\lambda_i = 3.34 \times 10^5$ J kg^{-1} 100% ice coverage of 2-m thickness	3.2×10^{21} J
Mountain glacier decrease (14)	1961–1997	3.7×10^3 km ³ decrease in mountain glacier ice volume	$\rho_i = 9.17 \times 10^{11}$ kg km^{-3} $\lambda_i = 3.34 \times 10^5$ J kg^{-1} 100% ice coverage of 2-m thickness	1.1×10^{21} J
Decrease in Northern Hemisphere sea ice extent (17)	1978–1996	Areal change based on satellite measurements	100% ice coverage of 2-m thickness	4.6×10^{19} J
Decrease in Arctic perennial sea ice volume (16)	1950s–1990s	40% decrease in sea ice thickness	Thickness of the melted sea ice = 1.3 m $\rho_i = 9.17 \times 10^{11}$ kg km^{-3} $\lambda_i = 3.34 \times 10^5$ J kg^{-1}	2.4×10^{19} J

REPORTS

that we are simply making "order-of-magnitude" estimates of these terms. Our results will demonstrate that for the purpose of determining which components of Earth's climate system dominated as sinks or sources of heat between the 1950s and 1990s, these assumptions are not critical. This is because the change in ocean heat content was by far the dominant sink of heat during this period.

Estimates of the melting of continental glaciers (Antarctica and Greenland) range from -1.8 to 1.8 mm of global sea level change per year (*J*). Using a value of 1.8 mm per year, the amount of heat required to melt continental glacier ice corresponding to this increase in sea level during a 41-year period is 8.1×10^{21} J.

The most recent estimates of mountain glacier variability document that the "loss of glacier volume has been more or less continuous since the 19th century" (*14*). During the 1961–1997 period, there was a loss of 3.7×10^3 km³ of mountain glacier volume. We compute a value of 1.1×10^{21} J for the amount of heat required to melt this volume of freshwater ice.

A 40% decrease in the thickness of perennial Arctic sea ice during the past 40 years has recently been estimated from ice draft measurements made from nuclear submarines (*15, 16*). Assuming an area of 6.85×10^6 km² for ice extent, the observed decrease in ice thickness of 1.3 m (*16*) corresponds to a decrease in ice volume of 8.9×10^9 km³. The amount of heat required to melt this volume of sea ice is 2.4×10^{19} J.

A net decrease in the areal coverage of Northern Hemisphere sea ice cover from 1978 to 1996 has been estimated from satellite measurements (*17*). Assuming that the area of decreased sea ice extent had 100% coverage of 2-m-thick sea ice, we estimate a total latent heat of fusion of 4.6×10^{19} J.

A decline in Antarctic sea ice extent has been suggested to have occurred between the early 1950s and the mid-1970s (*18*). The validity of this estimate has been questioned (*19*), and we cannot resolve this issue. As we shall see, this contribution, if real, represents only a minor contribution to Earth's heat balance during the 1955–96 period. Based on recently available historical whaling records, which provide a record of circumpolar sea ice extent, it is now estimated that the Antarctic sea ice boundary retreated poleward by an average of 2.8° of latitude between the 1950s and 1970s, whereupon the boundary stabilized. Assuming that the area of decreased sea ice extent had 100% coverage of 2-m-thick sea ice, a maximum of 3.2×10^{21} J of latent heat of fusion is associated with this change.

Our analysis of components of Earth's heat balance quantitatively demonstrates that during the latter half of the 20th century, changes in ocean heat content dominate the

changes in Earth's heat balance.

The observed increase in oceanic heat content is compared to changes in ocean heat content from a coupled model of Earth's climate system. The coupled ocean-atmosphere-ice model used, developed at the Geophysical Fluid Dynamics Laboratory (GFDL), is higher in spatial resolution than an earlier version used in many previous studies of climate variability and change (*20, 21*) but employs similar physics. The coupled model is global in domain and consists of GCMs of the atmosphere (spectral model with rhomboidal 30 truncation, corresponding to an approximate resolution of 3.75° longitude by 2.25° latitude, with 14 vertical levels) and ocean (1.875° longitude by 2.25° latitude, with 18 vertical levels). The model atmosphere and ocean communicate through fluxes of heat, water, and momentum at the air-sea interface. Flux adjustments (which did not vary interannually) are used to facilitate the simulation of a realistic mean state. Over oceanic regions, a thermodynamic sea ice model is used that includes the advection of ice by surface ocean currents.

Results are presented from two ensembles of integrations (each of which has three members). In the first ensemble (denoted GSSV), the radiative effects of the observed temporal variations in GHGs, sulfate aerosols, solar irradiance, and volcanic aerosols over the past century are included (*22*). The ensemble members differ in their initial conditions, which are chosen from widely separated points in a 900-year-long control integration. The second ensemble (denoted GS) differs from the first by omitting the radiative effects of changes in solar irradiance and volcanic aerosols, while retaining the effects of changes in GHGs and sulfate aerosols.

The global ocean heat content (calculated over the depth range from 0 to 3000 m) for the GSSV ensemble is shown in Fig. 1. Based on a linear trend, the simulated heat content increased by 19.7×10^{22} J over the period 1955 to 1996. This is in excellent agreement with the observed estimate (18.2×10^{22} J). However, it must be stressed that substantial uncertainties exist in the specification and parameterizations of the model radiative forcing, particularly with respect to the effects of sulfate aerosols and volcanic activity. In addition, the ocean heat content estimates are based on a data set characterized by coverage that varies with time (*23*). Thus, the close agreement between the simulated and observed ocean heat content increases must be evaluated in the light of these uncertainties. Nevertheless, this agreement is extremely encouraging with respect to the ability of the GFDL AOGCM to simulate the observed multidecadal changes in the heat balance of the ocean.

The second ensemble of integrations (GS) differs from the first by omitting the radiative

effects of changes in solar irradiance and volcanic aerosols. As shown in Fig. 1, the simulated increase of ocean heat content in GS is approximately 70% larger than in GSSV or than the observed estimate. Based on an additional set of experiments (*24*), the difference in ocean heat content increase between GSSV and GS is primarily due to the radiative effects of volcanic activity. The difference between GSSV and GS highlights the important role that volcanic activity appears to play in ocean heat content during the late 20th century. In the GSSV ensemble, volcanoes contributed an average global adjusted radiative forcing of -0.5 W m⁻² at the tropopause over the period 1960–1999 (*25*). This offsets an important fraction of the anthropogenic forcing during the same period.

It is important to evaluate whether the trend in simulated ocean heat content from the 1950s to the 1990s for ensemble GSSV (Fig. 1) could arise purely from internal variability of the coupled ocean-atmosphere system. To assess this, all possible 41-year trends were calculated in a 900-year integration of the coupled model without the radiative effects of changes in GHGs, sulfate aerosols, solar irradiance, and volcanic aerosols. No simulated 41-year trend in that integration (out of 860 possible 41-year trends) was as large as that simulated in any of the three ensemble members over the period 1955–1996, thereby demonstrating that the simulated trends in ocean heat content could not arise (in this model) solely from interactions within the ocean-atmosphere-ice system. The simulated trends require a sustained, positive thermal forcing, such as that expected from increasing concentrations of GHGs.

Although there is excellent agreement between the simulated and observed ocean heat content increases over the long term (from the 1950s to the 1990s), substantial differences exist on the decadal scale. In particular, simulated decadal variations are smaller in amplitude than the observed variations, and there are differences in phase. The causes of these differences need to be identified. Possible causes include an underestimation by the model of the internal variability of the ocean-atmosphere system on decadal scales and uncertainties in the estimates of past radiative forcing. Inadequacies in the ocean observational data may also play a role.

Our observational results make clear that each individual component of Earth's climate system that we have examined has warmed over the latter half of the 20th century and that the dominant change in heat content is associated with the warming of the world ocean. The agreement between our model results and observational estimates of ocean heat content supports the hypothesis that increases in radiative forcing are the source of the warming observed between 1955 and